

RESEARCH

Open Access



# Study on Flexural and Shear Behavior of UHPC Rhombus-Strip-Shaped Joint

Shuwen Deng<sup>1</sup>, Banfu Yan<sup>2\*</sup>, Lian Shen<sup>3</sup>, Mingxin Qin<sup>1</sup> and Yina Jia<sup>4</sup>

## Abstract

Accelerated bridge construction (ABC) has many advantages for bridge construction in modern society. While for ABC, the post-cast joint is always the weakest and most critical part. This paper presents a UHPC rhombus-strip-shaped (RSS) joint suitable for ABC. Several model tests were carried out to verify its resistance to flexural and shear. First, large-scale model tests are advanced to confirm its flexural properties. The results show that densified and welded joint interface rebars can significantly improve the ultimate bearing capacity and durability-based cracking stress of the RSS joint beams, and the ultimate bearing capacity can reach 90% of the complete beam. Then the shear-resistance tests were carried out. The results show that the UHPC RSS joint beam has excellent bending-shear mechanical properties and better ductility. Lastly, the ultimate flexural bearing capacity and shear-resistance capacity calculation methods were obtained.

**Keywords** Ultra-high performance concrete (UHPC), UHPC RSS joint, Flexural test, Shear test

## 1 Introduction

Nowadays, accelerated bridge construction (ABC) is the trend of bridge construction. The core concept of ABC is to use factory prefabrication and onsite assembly technology to reduce traffic impacts, onsite construction time, or weather-related time delays (Azizinamini, 2020; Ralls, 2007). ABC can also improve site constructability, total project delivery time, material quality and product durability, and work-zone safety for the travelling public and contractor personnel. The environmental impacts, existing roadway alignment impacts, utility relocations and right-of-way take could also be minimized (Culmo

et al., 2011). However, for ABC, the post-cast joint is the weakest and most critical part (Deng et al., 2020; Feng et al., 2018; Zhang et al., 2020).

The emergence of ultra-high-performance concrete (UHPC) brings more possibilities for bridge construction. UHPC is a class of cement-based material with excellent mechanical performance and durability (Graybeal, 2006; Graybeal et al., 2020). Graybeal (2006, 2009, 2010, 2011, 2012, 2014), Swenty and Graybeal (2013), Aaleti et al. (2011, 2014), Jung et al. (2014), Luo et al. (2019a, b), Pan et al. (2016), etc., have all studied the application of UHPC in bridge joints and achieved excellent results.

However, at present, the research on the post-cast UHPC joint mainly focuses on its flexural and tensile properties, and the research on its shearing properties is scarce. This paper proposes a UHPC rhombus-strip-shaped (RSS) joint suitable for ABC. Several model tests were carried out to verify its resistance to bending-tension and bending-shear, and the corresponding ultimate flexural capacity is proposed. At the same time, by reference to the existing criteria and theory, the shear-resistance capacity calculation method was found, providing a reference for applying RSS joint in bridge engineering.

Journal information: ISSN 1976-0485 / eISSN 2234-1315.

\*Correspondence:

Banfu Yan  
yanbanfu@gxu.edu.cn

<sup>1</sup> College of Water Resource & Civil Engineering, Hunan Agriculture University, Changsha, Hunan, China

<sup>2</sup> School of Civil Engineering and Architecture, Guangxi University, Nanning, Guangxi, China

<sup>3</sup> Department of Civil Engineering, Changsha University, Changsha, Hunan, China

<sup>4</sup> Sinopec Engineering Incorporation, Beijing, China

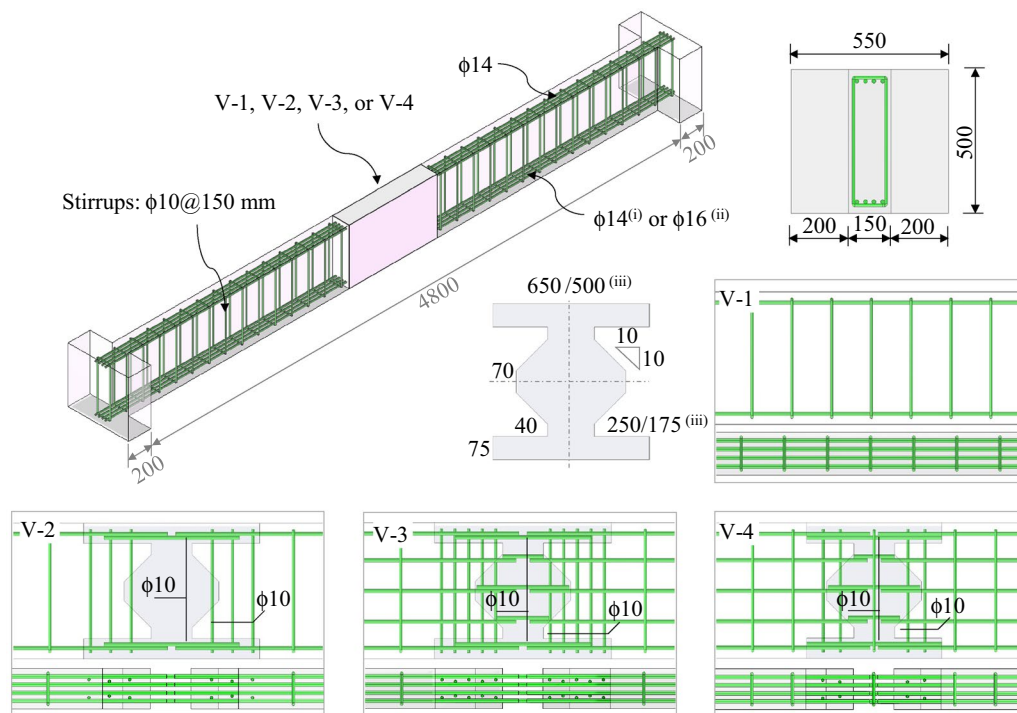


**Fig. 1** Design of large-size beam tests: (i)  $\phi 14$  is for V-1–V-3, (ii)  $\phi 16$  is for V-4, and (iii) 500 and 175 for V-4 (unit: mm)

**Table 1** Test specimen details

No.	Details	Joint reinforcement connection form	$\rho_c$ (%)	$\rho_i$
V-1	Complete beam without joint	–	1.64	1.64% L
V-2	Joint beam without waist reinforcement	Lap	3.28	1.64% L + 1.26% V
V-3	Joint beam with waist reinforcement	Lap	3.91	2.27% L + 2.09% V
V-4	Joint beam with waist reinforcement	Weld	4.41	2.52% L + 0.84% V

$\rho_c$  and  $\rho_i$  denote reinforcement ratio in the joint center and interface, respectively; L and V denote longitudinal and vertical reinforcement, respectively

## 2 RSS Joint Bending Resistance Evaluation

### 2.1 Test Introduction

The size of the specimens is 5.2 m in length, 0.5 m in height, and 0.15 m in width. The longitudinal and vertical steel bars were applied to increase the reinforcement ratio of the joint interface. As shown in Fig. 1, four beams were designed in the test: V-1 (beam without joint, for comparison), V-2 (RSS joint beam without central longitudinal rebar), V-3 (RSS joint beam within central longitudinal rebar), V-4 (RSS joint beam within welded central longitudinal rebar). The details of each beam are listed in Table 1.

UHPC150 (150 means the compressive strength of UHPC is above 150 MPa) was used in the prefabricated part of the test beam, and UHPC150 mixed with expansion agent (UHPC 150') was employed in the joint part.

**Table 2** Mechanical properties of UHPC in the test

UHPC type	$f_{cu}$ /MPa	$f_t$ /MPa	$f_i$ /MPa	$E_c$ /GPa
UHPC150	160.7	26.5	8.12	50.3
UHPC 150'	142.4	16.6	3.53	46

The round-straight steel fibers were used in the beam, within 13 mm length, 0.2 mm diameter, and 2.5% volume. The materials mechanical properties are demonstrated in Table 2. The manufacturing process of the test beam is shown in Fig. 2. Firstly, the prefabricated part of the test beam was cured by 90 °C high-temperature steam, then roughened the surface of the beam part where the joint will be poured, and then the joint part rebar was arranged. Lastly, the joint part UHPC was poured.



**Fig. 2** Manufacture process of test model: **a** roughening the surface, **b** splicing the pre-cast parts, and **c** natural curing the joint part

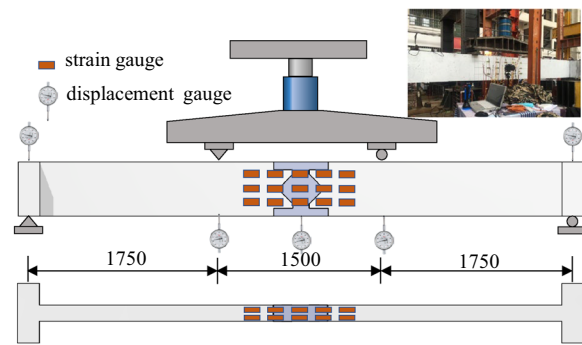


**Fig. 3** Loading and measuring scheme (unit: mm)

The loading scheme is shown in Fig. 3. The beam span is 5 m, and the shear-span ratio is 3.7. The deflection, strain of UHPC and reinforcement, and crack development were recorded during the test.

## 2.2 Test Results and Discussion

### 2.2.1 Failure Mode

As shown in Fig. 4, V-1 is the complete beam without joint, the failure characteristics are that the main crack continues to expand, and the dense secondary cracks grow together. Until the end of loading, the cracks were stopped in the middle of the test beam, and no crushing was found at the upper edge.

V-2 is the joint beam arranged with vertically crossing joint interface reinforcement. From Fig. 4b, the initial crack occurs in the middle of the span. As the load increases, the initial crack gradually deflects to the joint interface and forms a main crack. Multiple short and fine secondary cracks were generated in the pure bending area. When the beam failed, the longitudinal reinforcement yielded, the upper edge of the UHPC crushed, and only a few steel fibers were pulled out from the main crack gap.

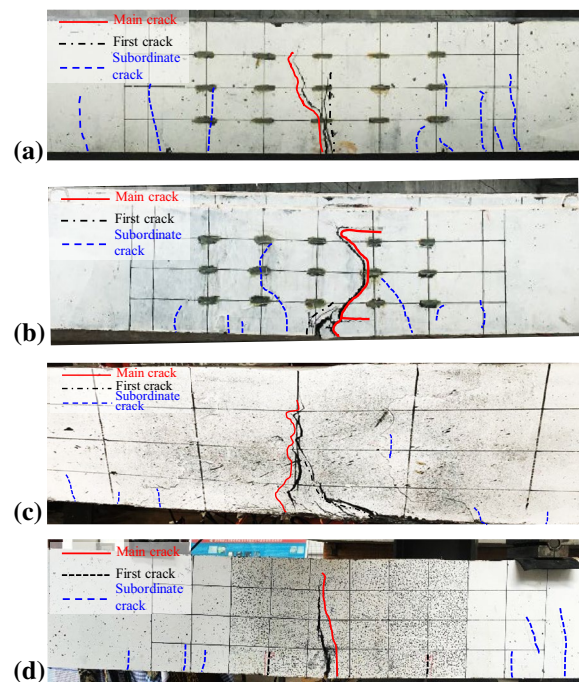


**Fig. 4** Failure mode: **a** beam without joint, **b** joint beam without middle rebar, **c** joint beam with middle rebar-I, **d** joint beam with middle rebar-II

V-3 and V-4 are also joint beams. In addition to configuring the same vertical reinforcement as V-2, intermediate reinforcements that pass through the joint interface were added. The V-4 joint connecting reinforcement was welded to the precast portion. As seen from Fig. 4c, d, the initial and the main cracks of the two beams were both in the midspan. Compared to V-2, adding intermediate reinforcements that cross the joint interface can effectively inhibit the development of interfacial cracks. Both beams exhibit similar failure patterns to the complete beam, that is, the main crack expands in the midspan

continuously, and the dense secondary cracks grow together. The welded beam V-4 performs better with less comprehensive reinforcement ratio of interface (V-2, V-3, and V-4 are 1.64% L+1.26% V=2.90%, 2.27% L+2.09% V=3.36%, and 2.52% L+0.84% V=4.36%, respectively). The welding method can better transfer the load in the joint beam with a relatively lower reinforcement ratio so

that the joint beam shows a failure form similar to the complete beam.

**2.2.2 Load–Displacement Curve and Crack Development**

During the test, the displacement development of each specimen was recorded. The load–displacement curves are summarized in Fig. 5, and the critical loads of the

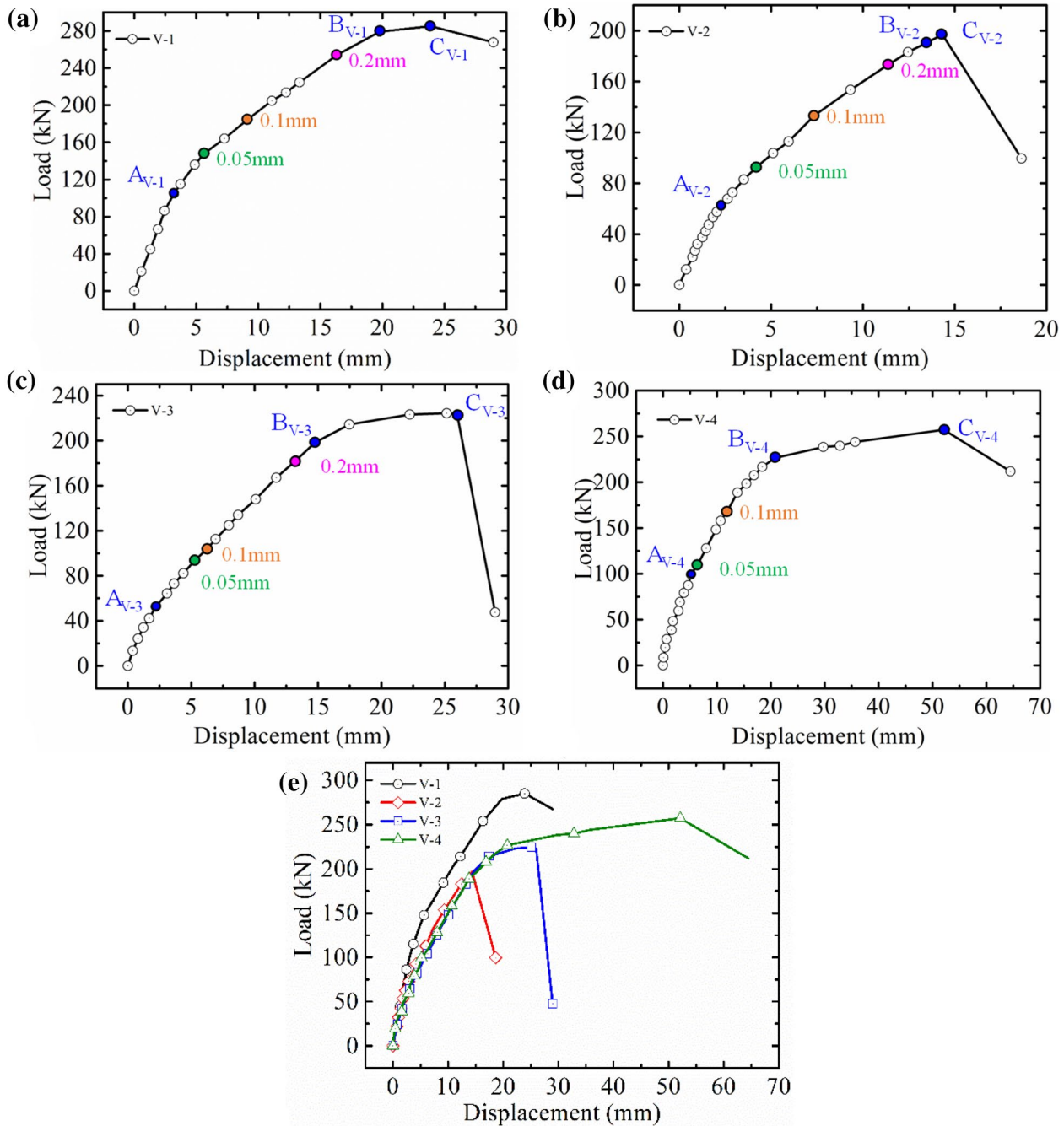


**Fig. 5** Load–displacement curves: **a** V-1, **b** V-2, **c** V-3, **d** V-4, and **e** comparison of four beams

beams are listed in Table 3. For more clarity, the data in Table 3 are plotted in Fig. 6. In the figure, “A” denotes the pre-cast part cracking; “B” means the beam reached yielding load; “C” demonstrates the beam reached ultimate load; “0.05 mm”, “0.1 mm” and “0.2 mm” indicate that the maximum crack width of the structure surface is 0.05 mm, 0.1 mm, and 0.2 mm, respectively.

The load–displacement curves can be roughly divided into the following stages: (i) elastic stage (O–A): the load–displacement curve is approximately linear in this stage. Although the joint interface of V-2 and V-4 were firstly cracked in this stage, it did not have a significant impact on the overall stiffness of the structure; (ii) crack development stage (A–B or A–C): a large number of cracks were developed in this stage. The existing cracks in the matrix and interface developed rapidly; (iii) yield stage (B–C): among the four specimens, only V-3 and V-4 had apparently yield platforms, and the rest were breaking soon after the rebar was yielded; (iv) structural failure (after C): at this stage, the deformation of the specimen increased rapidly, and the load could not be applied, then the tests were terminated.

As shown in Table 3, Figs. 5 and 6, the slope of the load–displacement curve (stiffness) and typical load

values of the specimen are significantly improved when the reinforcement ratio of the joint interface is increased. It can be seen from Fig. 5e that the stiffness of the joint beams is similar to that of the complete beam, wherein V-4 has better ductility, and V-3 has similar ductility to the complete beam V-1. Compared with the complete beam V-1, the initial cracking strength of the joint beams are increased to 0.55–0.84 times, the initial cracking strength of the beam matrix are 0.5–0.78 times, and the failure loads can be reached as 0.69–0.9 times. It can be seen from Fig. 6b that the load dispersion corresponding to each critical cracking point of the four beams is relatively small, and V-4 shows better cracking resistance strength than V-2 and V-3.

Therefore, it is proved that increasing the reinforcement ratio and welding the joint connecting reinforcement can significantly improve the load transfer efficiency, making the joint matrix has higher strength.

### 2.2.3 Durability-Based Cracking Stress

According to Rafiee (2012), cracks do not affect the durability of the UHPC when the maximum crack width does not exceed 0.05 mm. In the French code, the maximum requirement of crack width is 0.05 mm. Thus, when the

**Table 3** Test beam critical loads

No.	Failure/kN	Interface cracking/kN	Matrix cracking/kN	$F_{V-i}/F_{V-1}$	$F_{0.05mm}/kN$	$F_{0.1mm}/kN$	$F_{0.2mm}/kN$
V-1	286.1	–	87.6	1	147.94	184.46	253.90
V-2	197.4	53.4	48.4	0.69	92.62	133.23	173.38
V-3	225.4	73.5	43.4	0.79	93.55	103.83	182.47
V-4	256.2	47.9	68.7	0.90	109.13	167.81	–

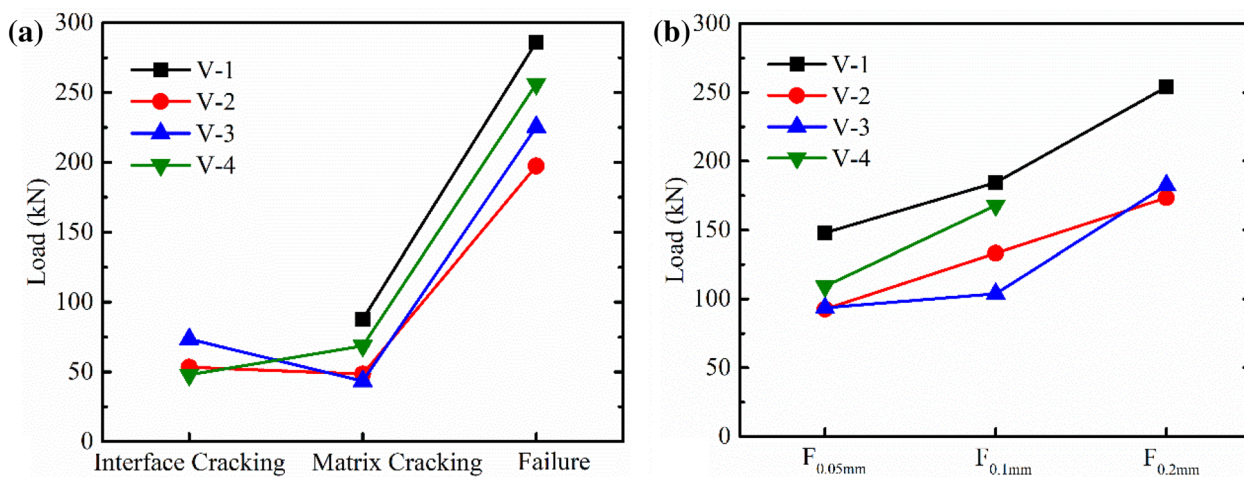


**Fig. 6** Critical load of the test beam: **a** interface cracking, matrix cracking and failure load; **b** the loads of critical crack width

**Table 4** Durability-based cracking stress

No.	$\sigma_{0.05}/\text{MPa}$	$\sigma_{0.1}/\sigma_{0.1}$	Crack location
V-1	20.71	1	Matrix
V-2	12.97	0.63	Interface
V-3	13.10	0.63	Joint matrix
V-4	15.28	0.74	Joint matrix

crack width of the UHPC is less than 0.05 mm, durability can be guaranteed. Luo et al. (2019a, b) conducted bending tests on 40 steel-UHPC composite beam plates. The results show that when the maximum crack width of UHPC reaches 0.05 mm, the test beam is still in the early stage of the crack expansion. When the applied load reaches 76.7%–86% of the ultimate load, the strain distribution along with the test beam’s height still meets the plane cross-sectional assumption.

In addition, in practical engineering, when the maximum crack width on the concrete surface is less than 0.05 mm, it is challenging to be observed with the naked eye. Thus, for the UHPC structure, we define the allowable crack width based on durability as 0.05 mm. The corresponding load and stress can be defined as Durability-based cracking load and stress, respectively.

The nominal cracking stress can be calculated based on:

$$\sigma = M_d y / I,$$

where  $M_d$  is the external bending moment,  $y$  is the distance from the section’s neutral axis to the cracking surface, and  $I$  is the second-moment area of the cross-section. The nominal cracking stress of each beam is calculated and listed in Table 4.

In Table 4,  $\sigma_{0.05}$  denotes the nominal stress corresponding to crack width reaching 0.05 mm, and  $\sigma_{0.1}/\sigma_{0.1}$  denotes ratio of  $\sigma_{0.05}$  of each beam to V-1. As shown in the table, the durability-based cracking stress of the joint beams is only 0.63–0.74 times the complete one. V-3 and V-4 cracked in the middle of the joint, indicating that adding waist reinforcement can effectively reduce the risk of interface cracking. It can be seen from the test results of V-4 that weld has the advantage compared with the overlap in terms of the mechanical property. While for actual engineering, welding may cause many problems, such as difficult construction and prolonged on-site time. Therefore, the test results of V-3 applying lap details are also acceptable.

**2.3 The Preliminary Summary of the Test**

According to the above tests, the densified reinforcement and welded joint connection rebar can significantly

improve the ultimate bearing capacity and durability-based cracking strength of post-cast joints. Compared with V-2 and V-3, although the corresponding strength was the same when the crack width reached 0.05 mm, their failure mode (Fig. 4) showed that there was no doubt that the densified-lap beam V-3 strengthened by intermediate reinforcement has more advantages. For V-4, the ultimate bearing capacity can reach 90% of the complete specimen (V-1) in terms of a similar reinforcement ratio and change the connection mode of welding. However, welding may increase the on-site construction difficulty and time. Therefore, densified-lap beam V-3 is more recommended for practical projects.

**2.4 Ultimate Flexural Capacity of RSS Jointed Beam**

The most significant difference between UHPC structure and ordinary concrete in the flexural capacity calculation is that the tensile strength of UHPC in the tensile zone cannot be ignored. According to the test phenomenon and results, assuming that the lower rebar reached the yield strength and the compression zone height is  $x$ , the calculation formulas were as follows (1)–(2), and the calculation diagram was as shown in Fig. 7:

$$\sigma_{st} A_{st} + \frac{1}{2} f_t (h_0 - x - h_t) b + f_t b h_t - \left( \frac{1}{2} \sigma_c b x + \sigma_{sc} A_{sc} \right) = 0, \tag{1}$$

$$M_u = \frac{1}{3} \sigma_c b x^2 + \sigma_{sc} A_{sc} (x - a_s) + \sigma_{st} A_{st} (h_0 - x) + f_t b h_t \left( h_0 - x - \frac{1}{2} h_t \right). \tag{2}$$

In the formula, the  $\sigma_{st}$ ,  $A_{st}$  and  $A_{sc}$  denote that the yield strength of the rebar, the area of the rebar part contributed to tensile and compressive, respectively;  $f_t$  and  $\sigma_c$  respectively;  $h_0$  is the effective depth of the beam;  $h_t$  is the height of the strip;  $b$  is the width of the beam;  $x$  is the depth of the compressive part;  $a_s$  is the cover depth of the UHPC.

Thus, the calculated value of ultimate bearing capacity of V-4 can be obtained (243.5 kN m), which is about 95% of the test value (256.2 kN m).

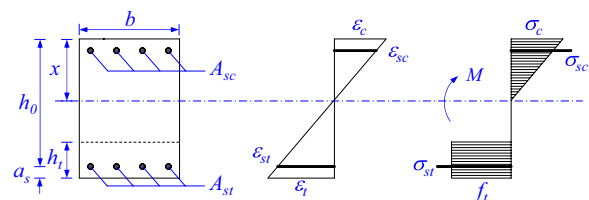


**Fig. 7** Ultimate bearing capacity calculate diagram

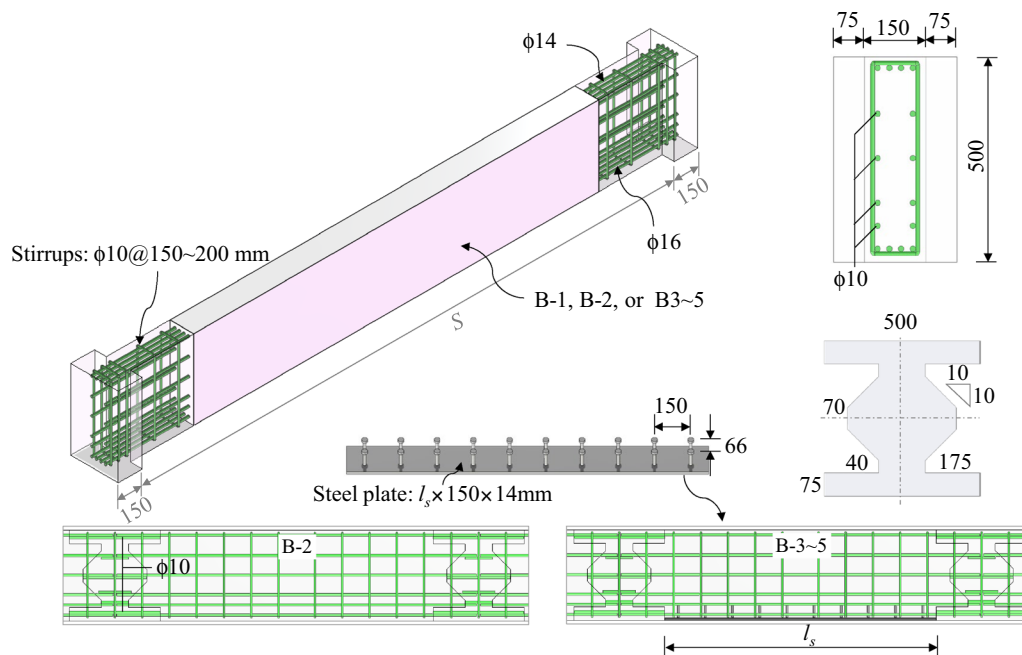


**Fig. 8** Schematic diagram of the RSS joint test beam:  $S$  for B-1, B-2, and B-5 are 3350 mm, for B-3 is 1700 mm, for B-4 is 2350 mm;  $l_s$  for B-3 is 600, for B-4 is 1000, for B-5 is 1500. (unit: mm)

**Table 5** Shear-resistance test model details

No.	Joint location	Span/m	Shear-to-span ratio	Effective height/m
B-1	Complete beam	3.5	3.14	470
B-2	Flexural-shear section	3.5	3.14	470
B-3	Flexural-shear section	1.85	1.41	470
B-4	Flexural-shear section	2.5	2.09	470
B-5	Flexural-shear section	3.5	3.14	470

### 3 RSS Joint Shear Performance Evaluation

#### 3.1 Test Introduction

Five beams were designed for test, including one complete beam (B1) and four joint beams (B2–B5) with the joint setting in the flexural-shear section. In order to

prevent the beams from being destroyed by flexure in advance, three beams (B3–B5) were reinforced with steel plates in the middle span. The beam sections are all rectangles with the size of 0.5 m×0.15 m (height×width). The detail of each specimen is shown in Fig. 8 and Table 5.

The manufacturing processes are shown in Fig. 9. The materials used in the test are the same as those in the previous section. The loading and measuring scheme is displayed in Fig. 10. The deflection, strain of UHPC and reinforcement, and crack development were recorded during the test.

#### 3.2 Test Results and Discussion

##### 3.2.1 Load-Displacement Curve and Crack Propagation

The load-displacement curves of test beams are drawn in Fig. 11. The corresponding cracking development



**Fig. 9** The production process of the specimens: **a** fabrication of formwork and reinforcement, **b** pouring pre-cast part UHPC, **c** joint splicing, and **d** pouring post-cast joint part UHPC

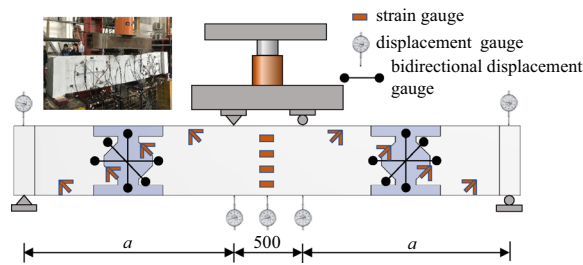


**Fig. 10** The loading and measuring details:  $a$  for B-1, B-2, and B-5 is 1500 mm, for B-3 is 675 mm, for B-4 is 1000 mm. (unit: mm)

is shown in Fig. 12. In the figure, the meaning of A, B and C is the same as Fig. 2. The load–displacement curves of all the beams can be divided into (i) elastic stage (before A), the beams have no crack and no stiffness change; (ii) crack development stage (A–B), the cracks appear one after the other, and quickly become more variable, longer and wider; (iii) yield stage (B–C), the reinforcement in the specimen gradually yield; and (iv) failure stage (after C), the test beam failed, and the curves declined.

It can be seen from Fig. 11f that compared with B-1 and B-2, the overall stiffness and bearing capacity of the test beam reinforced by steel plates (B-3–B-5) are significantly improved. Due to the reinforcement at the waist of B-2, the ultimate bearing capacity was significantly increased. Furthermore, according to the test results of B-3–B-5: when the shear–span ratio increases from 1.41, 2.09 to 3.14, the ultimate load decreases by 8.4% and 20.8%, respectively.

### 3.2.2 Discussion

According to the test results of B-1 and B-2, the main cracks of both specimens finally appeared on the bottom surface between two loading points. The longitudinal rebars at the bottom yielded when the beam failed. There were multiple oblique cracks in the shear span section. B-2 has obvious oblique cracks along with the joint interface. The bearing capacities of the two beams are similar, and the ductility of the B-2 is better than that of the complete beam B-1, indicating that the bending and shear behavior of the RSS joint is excellent.

From the test results of B-3–B-5, two failure modes appeared on the different shear–span ratios (1.41–3.14) of the RSS joint beam: shear-compression failure occurs when the shear–span ratio is 2.09 and 3.14, and diagonal compression failure occurs when the shear–span ratio is 1.41. With the increase of the shear–span ratio, the ductility of beams increases and the ultimate bearing capacity decreases gradually.

### 3.3 Theoretical Formula of the Shear-Resistance Capacity

Due to the small number of test samples, this paper selects the existing specifications and theoretical calculation formula to compare the model test results to find a more accurate method to calculate the shear-resistance capacity of the UHPC RSS joint beam. The calculation formula used in this paper includes: (i) technical specification for fiber reinforced concrete structures (CECS38: 2004) (CECS, 2004; Chengkui & Guofan, 2004); (ii) Ultra High Performance Fiber Reinforced Concretes Interim Recommendations (SETRA-AFGC2016) (AFNOR, 2016); (iii) upper bound theory of plasticity (Nielsen, 1963, 1967); (iv) modified compression field theory (Vecchio & Collins, 1986); and (v) Truss–Arch model (Kim et al., 1998; Leonardt, 1965). In the following calculation, the mechanical properties of UHPC in the test were applied.

#### 3.3.1 CECS38: 2004 (CECS, 2004; Chengkui & Guofan, 2004)

$$V_u = V_{fc} + V_{sv}, \tag{3}$$

$$V_{fc} = V_c(1 + \beta_v \lambda_f), \tag{4}$$

$$V_{sv} = f_{yv} \frac{A_{sv}}{s} h_0. \tag{5}$$

In the above formulas,  $V_{fc}$  is the shear-bearing capacity contributed by steel fiber reinforced concrete;  $V_c$  is the resistance of concrete without steel fiber;  $\beta_v$  is improvement factor of steel fiber on structural bearing capacity;  $\lambda_f$  is the characteristic value of steel fiber;  $f_{yv}$  is stirrup yield strength;  $A_{sv}$  is stirrup cross-sectional area;  $s$  is stirrup spacing;  $h_0$  is effective beam height.

#### 3.3.2 SETRA-AFGC2016 (AFNOR, 2016)

$$V_{Rd} = V_{Rd,c} + V_{Rd,f} + V_{Rd,s}, \tag{6}$$

$$V_{Rd,c} = \frac{0.21}{\gamma_{cf} \gamma_E} k f_{ck}^{1/2} b_w d, \tag{7}$$

$$V_{Rd,f} = \frac{A_{fv} \sigma_{Rd,f}}{\tan \theta}, \tag{8}$$

$$V_{Rd,s} = \frac{A_{sw}}{s} z f_{ywd} \cot \theta. \tag{9}$$

In the above formulas,  $V_{Rd,c}$ ,  $V_{Rd,f}$  and  $V_{Rd,s}$  are the shear-bearing capacity contributed by UHPC, steel fiber, and stirrups, respectively;  $\gamma_{cf}$ ,  $\gamma_E$  is the safety

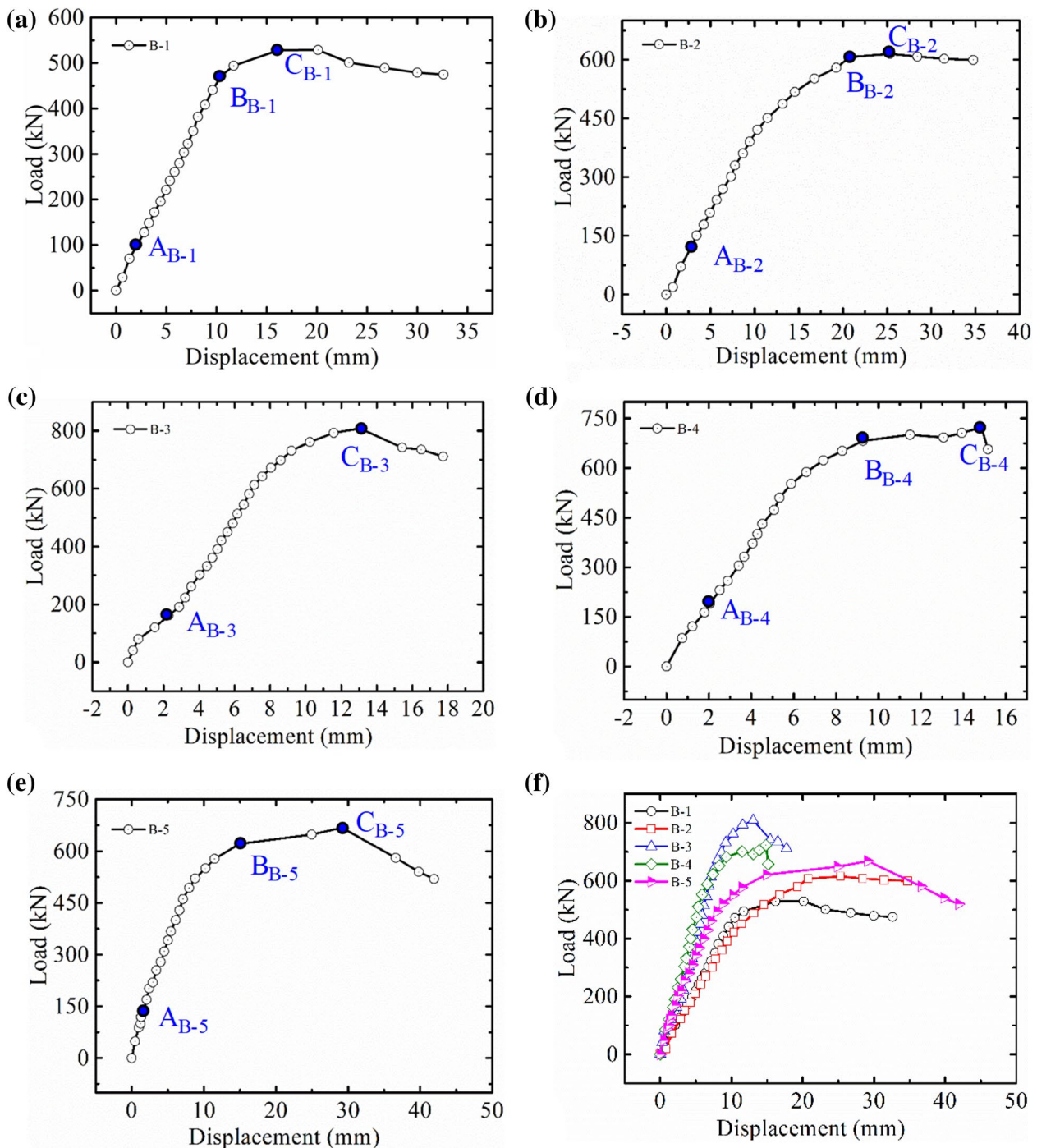


**Fig. 11** The displacement curve of the load (B-1–B-5): **a** B-1, **b** B-2, **c** B-3, **d** B-4, and **e** B-5, **f** comparison of five beams

factor for the strength of UHPC material;  $k$  is pre-stressed influence coefficient;  $f_{ck}$  standard value of axial compressive strength of UHPC cylinder;  $b_w$  and  $d$  are the width and effective height of the beam section, respectively;  $A_{fv}$  is the effective area of fiber distribution;  $\sigma_{Rd,f}$  is the residual tensile strength of UHPC after

cracking;  $\theta$  is the angle between the principal compressive stress and the horizontal axis of the beam;  $A_{sw}$  is stirrup cross-sectional area;  $z$  is the distance between the top and bottom reinforcement points;  $f_{ywd}$  is the yield strength of stirrups.

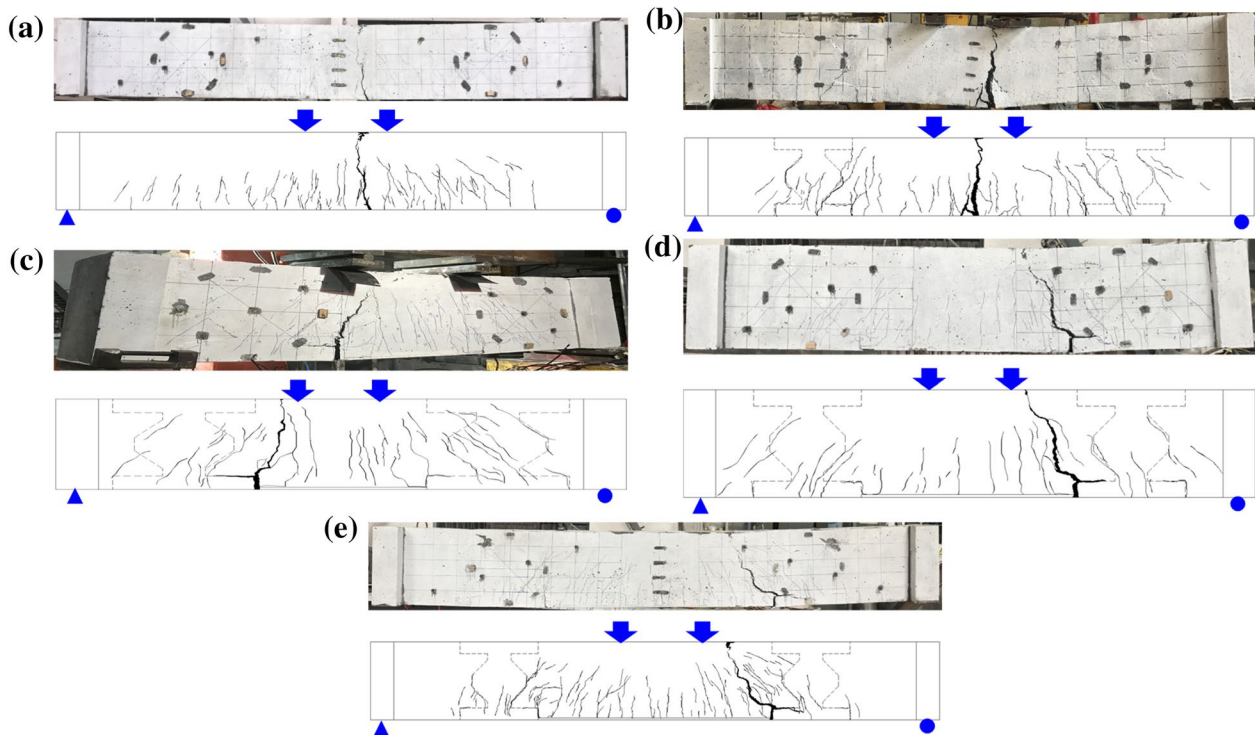


**Fig. 12** Crack development of specimen: **a** B-1, **b** B-2, **c** B-3, **d** B-4, and **e** B-5

**3.3.3 Upper Bound Theory of Plasticity (Nielsen, 1963, 1967)**

In plasticity theory, steel bars and concrete are ideal rigid-plastic materials. When the yield criterion is selected, the upper and lower bounds of the equation can be solved using the upper and lower bound theorem. Since the lower bound solution is often difficult to obtain, the upper bound solution is usually used as the shear-resistance capacity of the beam. Therefore, based on the upper bound theory of plasticity, Voo (Jin et al., 2015; Kwak et al., 2002; Lei et al., 2006) proposed to use the following formula to calculate the shear capacity of UHPC beams:

$$V_u = \frac{1}{2} \zeta f_c b h \left( \sqrt{1 + \left( \frac{0.772a}{h} \right)^2} - \frac{0.772a}{h} \right). \quad (10)$$

In the formula,  $\zeta$  is the influence factor for section size;  $f_c$  is the effective concrete strength;  $b$  and  $h$  are the width and depth of the section, respectively;  $a$  is the length of the beam shear-span part.

**3.3.4 Modified Compression Field Theory (Vecchio & Collins, 1986)**

In this method, the load–deformation relationship of the shear inclined section can be iteratively obtained by using the equilibrium condition, constitutive relationship and deformation coordination relationship of stirrups

and obliquely cracked concrete structures. Because the mechanical properties of UHPC mixed with steel fiber are quite different from those of ordinary concrete, this paper adopts the improved limit equilibrium theory for calculation (Liang & Wang, 2019; Liang et al., 2018; Xu & Deng, 2015; Xu et al., 2014):

$$V_u = V_c + V_t + V_s, \quad (11)$$

$$V_c = 0.236 \alpha_1 b f_c \left( x_n - 0.0623 \frac{\varepsilon_0 (d - x_n)}{\varepsilon_{sx}} \right), \quad (12)$$

$$V_t = \beta \sqrt{f_c} b (d - x_n), \quad (13)$$

$$V_s = (\rho_v f_{yv} \cot \theta + f_{tp} \cot \theta) b (d - x_n). \quad (14)$$

In the above formulas,  $V_c$  is the shear-resistance contributed by UHPC compression zone;  $V_t$  is the shear-resistance contributed by the friction of UHPC tension zone;  $V_s$  is the shear-resistance from stirrups and steel fiber bridging between cracks;  $\alpha_1=1.1$ , is compression influence coefficient;  $b$  is the width of the beam;  $f_c$  is the compressive strength of UHPC;  $d$  is effective depth;  $x_n$  is neutral axis height;  $\varepsilon_0$  is the strain at peak compressive stress of UHPC;  $\varepsilon_{sx}$  is the strain of tensile longitudinal rebars;  $\rho_v$  is

the stirrups ratio;  $f_{yv}$  is the yield strength of stirrups;  $f_{tp}$  is the tensile stress of the steel fibers between the cracks.

**3.3.5 Truss–Arch Model (Kim et al., 1998; Leondardt, 1965)**

According to the research of Ma et al. (2017), Xu and Gao (2000), Xing and Liang (2015), the longitudinal bars and stirrups in the specimens can be regarded as tension bars, the concrete as diagonal compression bars. As shown in Fig. 13. The shear force can be transferred to the support by the above trusses.  $N$  is the applied load, and  $z$  is the distance between the upper and lower trusses. The shear-resistance capacity contributed by UHPC in the tensile zone and the shear force borne by the UHPC arch in the compression zone are as follows:

$$V_u = V_f + V_s + V_a, \tag{15}$$

$$V_f = f_t b z \cot \theta, \tag{16}$$

$$V_s = \rho_s f_y b z \cot \theta, \tag{17}$$

$$V_a = \frac{1}{2} \sqrt{\lambda^2 + 4 \sin^2 \theta \cos^2 \theta} (1 - \eta_2) v f_c b d. \tag{18}$$

In which,  $V_f$  is shear resistance contributed by UHPC in tension zone;  $V_s$  is the shear resistance from the stirrups;  $V_a$  is the shear force of UHPC arch in compression zone;  $f_t$  is the tensile strength of UHPC;  $b$  is the width of the beam;  $f_y$  is the yield strength of the rebar;  $\lambda$  is shear-span ratio;  $\eta_2$  is the coefficients related to the difference in the inclination of the concrete oblique struts and the strength of the material;  $v$  is the softening factor of UHPC;  $d$  is the effective depth of the beam.

**3.3.6 Calculating Results**

The above calculation results are listed in Table 6. According to the results, all five methods can accurately predict the shear-resistance capacity of UHPC RSS joint beams to a certain extent. When using the CECS38:2004 recommended method and modified compression field theory, the average calculated values are slightly higher than the experimental results. When the SETRA-AFGC2016 recommended method, the upper bound

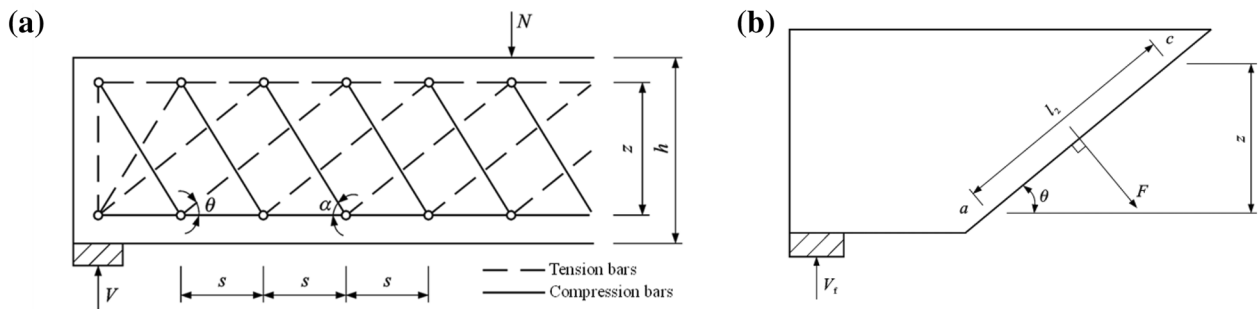


**Fig. 13** The calculation scheme of truss–arch model: **a** calculation model, **b** force in tension area

**Table 6** The results of the shearing test and the theoretical results (unit: kN)

No.	B-3	B-4	B-5	Average	Standard deviation	Variation coefficient
Ex	667	723	806	732	–	–
Pr.1	1018.8	849	636.8	834.9	0.25	27.56%
Ex./Pr.1	0.65	0.85	1.27	0.92		
Pr.2	883.8	736.5	552.4	724.2	0.29	27.56%
Ex./Pr.2	0.75	0.98	1.46	1.07		
Pr.3	997.6	733.1	512.7	747.8	0.37	34.79%
Ex./Pr.3	0.67	0.99	1.57	1.08		
Pr.4	883.5	842.8	704.8	810.4	0.16	17.89%
Ex./Pr.4	0.75	0.86	1.14	0.92		
Pr.5	907.8	687.2	499	698	0.36	32.11%
Ex./Pr. 5	0.73	1.05	1.62	1.13		

theory of plasticity and the truss–arch model are used, the average calculated values are slightly lower than the experimental results, and there is a certain safety margin. The plastic upper limit theory and the truss–arch model are discrete, while the limit equilibrium theory is the least discrete.

In general, the modified compression field theory to estimate the UHPC RSS joint beam results in line with the best. In addition, when the shear–span ratio is greater than 3, the calculated results are conservative, and when the shear–span ratio is less than 1.5, the calculated results are insecure. When the shear–span ratio is between 1.5 and 3, the calculated results are in good agreement with the measured values.

#### 4 Conclusion

This paper proposes a post-cast UHPC RSS joint suitable for assembled UHPC bridge structure. Bending tests and flexural–shear tests are carried out to verify its flexural and shear properties. The following work is completed, and corresponding conclusions can be drawn:

1. During the process of the bending test, it was found that good results could be obtained after the densified and welded connection rebar of the joint. The ultimate strength and the durability-based cracking stress of the densified-lap beam could reach 79% and 63% of the complete one. In contrast, the densified-weld beam is 90% and 74%.
2. Through the theoretical analysis of the flexural test, the formula for calculating the flexural bearing capacity of the UHPC RSS joint beam was obtained, and the estimated value is 95% of the test result.
3. According to the bending-shear test, UHPC RSS joint beam has excellent bending-shear mechanical properties and better ductility compared with the complete beam. By changing the shear–span ratio, it can be found that shear-compression failure occurs when the shear–span ratio is 2.09 and 3.14, and baroclinic failure occurs when the shear–span ratio is 1.41. With the increase of the shear–span ratio, the ductility of specimens increases gradually, and the ultimate bearing capacity decreases gradually.
4. The existing specifications and theory are performed to predict the test results. The results show that the limit equilibrium theory presents good agreement with the test results.

#### Acknowledgements

The authors acknowledge the financial support received from the Natural Science Foundation of China (No. 52108211), Hunan Provincial Department of Education (No. 21B0188), and Natural Science Foundation of Hunan Province (No. 2022JJ40186).

#### Author contributions

SD: conceptualization, methodology, software, funding acquisition, writing—original draft. BY: supervision, resources, project administration, review. LS: validation, data curation, software, review. MQ: picture, writing—review draft. YJ: experimental test.

#### Funding

This investigation was supported by the following funders, and their role of the funding body was declared as follows: (1) Natural Science Foundation of China (No. 52108211); (2) Hunan Provincial Department of Education (No. 21B0188); and (3) Natural Science Foundation of Hunan Province (No. 2022JJ40186).

#### Availability of data and materials

All data, models, or code that support the findings of this study are available from the corresponding author upon reasonable request.

#### Declarations

#### Competing interests

The authors declare that they have no known competing financial interests or personal relationships that could have appeared to influence the work reported in this paper.

Received: 16 June 2022 Accepted: 2 September 2023

Published online: 03 November 2023

#### References

- Aaleti, S., Honarvar, E., & Sritharan, S., et al. 2014. Structural characterization of UHPC waffle bridge deck and connections (No. IHRB Project TR-614). Iowa State University. Institute for Transportation.
- Aaleti, S., Sritharan, S., & Bierwagen, D., et al. 2011. Experimental evaluation of structural behavior of precast UHPC waffle bridge deck panels and connections. In: *Proceedings of the 90th annual meeting*. pp. 23–27.
- Association Française de Normalisation. (2016). *National addition to Eurocode 2—Design of concrete structures: Specific rules for ultra-high performance fibre-reinforced concrete (UHPC)*. Association Française de Normalisation.
- Azizinamini, A. (2020). Accelerated bridge construction. *Journal of Bridge Engineering*, 25(12), 02020002. [https://doi.org/10.1061/\(ASCE\)BE.1943-5592.0001643](https://doi.org/10.1061/(ASCE)BE.1943-5592.0001643).
- CECS. (2004). *Technical specification for fiber reinforced concrete structures*. China Planning Press.
- Chengkui, H., & Guofan, Z. (2005). Introduction of technical specification for fiber reinforced concrete structures (CECS38: 2004). *Building Structure*, 35(4), 74–79.
- Culmo, M. P., Lord, B., Huie, M., et al. (2011). *Accelerated bridge construction: Experience in design, fabrication and erection of prefabricated bridge elements and systems: Final manual*. Federal Highway Administration, Office of Bridge Technology.
- Deng, S., Shao, X., Yan, B., et al. (2020). On flexural performance of girder-to-girder wet joint for lightweight steel-UHPC composite bridge. *Applied Sciences*, 10(4), 1335.
- Feng, D. C., Wu, G., & Lu, Y. (2018). Finite element modelling approach for precast reinforced concrete beam-to-column connections under cyclic loading. *Engineering Structures*, 174, 49–66.
- Graybeal, B. A. (2006). *Material property characterization of ultra-high performance concrete*. Federal Highway Administration, Office of Infrastructure Research and Development.
- Graybeal, B. A. (2009). *Structural behavior of a 2nd generation ultra-high performance concrete pi-girder*. Federal Highway Administration, Office of Infrastructure Research and Development.
- Graybeal, B. A. (2010). *Behavior of field-cast ultra-high performance concrete bridge deck connections under cyclic and static structural loading*. Federal Highway Administration.
- Graybeal, B. A. (2011). Fatigue response in bridge deck connection composed of field-cast ultra-high-performance concrete. *Transportation Research Record*, 2251(1), 93–100.

- Graybeal, B. A. (2012). *Ultra-high performance concrete composite connections for precast concrete bridge decks*. Federal Highway Administration, Office of Infrastructure Research and Development.
- Graybeal, B. (2014). *Design and construction of field-cast UHPC connection*. Federal Highway Administration.
- Graybeal, B., Brühwiler, E., Kim, B. S., et al. (2020). International perspective on UHPC in bridge engineering. *Journal of Bridge Engineering*, 25(11), 04020094.
- Jin, L., Zhou, J., Li, Y., et al. (2015). Experimental study on shear bearing capacity of RPC beams with high strength reinforcement. *Journal of Building Structures*, 36(52), 9.
- Jung, K., Park, S. Y., Kim, S. T., et al. (2014). A study on the flexural performance of UHPC Precast Deck-joint interface by the exposure of steel fiber. *Engineering*, 6(13), 1000.
- Kim, D., Kim, W., & White, R. N. (1998). Prediction of reinforcement tension produced by arch action in RC beams. *Journal of Structural Engineering*, 124(6), 611–622.
- Kwak, Y. K., Eberhard, M. O., Kim, W. S., et al. (2002). Shear strength of steel fiber-reinforced concrete beams without stirrups. *ACI Structural Journal*, 99(4), 530–538.
- Lei, V. Y., Foster, S. J., & Ian, G. R. (2006). Shear strength of fiber reinforced reactive powder concrete prestressed girders without stirrups. *Journal of Advanced Concrete Technology*, 4(1), 123–132.
- Leonhardt, F. (1965). Reducing the shear reinforcement in reinforced concrete beams and slabs. *Magazine of Concrete Research*, 17(53), 187–198.
- Liang, X., & Wang, Z. (2019). Shear capacity analysis of ultra-high-performance concrete beams based on the improved MCFT. *Industrial Construction*, 1, 49.
- Liang, X., Wang, Z., Yu, J., et al. (2018). Study on shear behavior and shear bearing capacity of UHPC beams with stirrups. *China Civil Engineering Journal*, 51(10), 12.
- Luo, J., Shao, X., Cao, J., et al. (2019a). Transverse bending behavior of the steel-UHPC lightweight composite deck: Orthogonal test and analysis. *Journal of Constructional Steel Research*, 162, 105708.
- Luo, J., Shao, X., Fan, W., et al. (2019b). Flexural cracking behavior and crack width predictions of composite (steel+ UHPC) lightweight deck system. *Engineering Structures*, 194, 120–137.
- Ma, X., Chen, B., Yang, Y., et al. (2017). Calculation method of shear capacity of R-UHPC beam. *Journal of Traffic and Transportation Engineering*, 17(5), 16–26.
- Nielsen, M. P. 1963. Yield conditions for reinforced concrete shells in the membrane state. Proceedings. pp. 1030–1040.
- Nielsen, M. P. (1967). Shear reinforcement in reinforced concrete beams. *Bygningstatiske Meddelelser*, 38(2), 33.
- Pan, W. H., Fan, J. S., Nie, J. G., et al. (2016). Experimental study on tensile behavior of wet joints in a prefabricated composite deck system composed of orthotropic steel deck and ultrathin reactive-powder concrete layer. *Journal of Bridge Engineering*, 21(10), 04016064.
- Rafiee, A. (2012). *Computer modeling and investigation on the steel corrosion in cracked ultra high performance concrete*. Kassel University Press GmbH.
- Ralls, M. L. (2007). Accelerated bridge construction. *ASPIRE*. Springer. p. 16–20.
- Swenty, M. K., & Graybeal, B. A. (2013). *Material characterization of field-cast connection grouts*. Federal Highway Administration, Office of Infrastructure Research and Development.
- Vecchio, F. J., & Collins, M. P. (1986). The modified compression-field theory for reinforced concrete elements subjected to shear. *ACI Journal*, 83(2), 219–231.
- Xing, P., & Liang, X. (2015). Shear capacity analysis of fiber reinforced concrete beams based on truss-arch model. *Building S*, 10, 5.
- Xu, H., & Deng, Z. (2015). Shear bearing capacity of ultra-high performance concrete beams. *Journal of Huazhong University of Science and Technology (nature Science Edition)*, 43(7), 24–28.
- Xu, H., Deng, Z., Chen, C., et al. (2014). Experimental study on shear strength of ultra-high performance fiber reinforced concrete beams. *China Civil Engineering Journal*, 47, 12.
- Xu, Y., & Gao, W. (2000). Development of Research on Concrete Softening Constitutive Relation. *Journal of Shijiazhuang Railway Institute*, 13(2), 34–38.
- Zhang, Z., Wang, F., & Chi, B. (2020). Seismic performance of shear-critical pre-fabricated reinforced masonry shear walls with innovative vertical joint connections. *Engineering Structures*, 219, 110958.

## Publisher's Note

Springer Nature remains neutral with regard to jurisdictional claims in published maps and institutional affiliations.

**Shuwen Deng**, PhD, College of Water Resource & Civil Engineering, Hunan Agriculture University, Changsha, Hunan, China

**Banfu Yan**, Professor, School of Civil Engineering and Architecture, Guangxi University, Nanning, Guangxi, China

**Lian Shen**, Professor, Department of Civil Engineering, Changsha University, Changsha, Hunan, China

**Mingxin Qin** BE. College of Water Resource & Civil Engineering, Hunan Agriculture University, Changsha, Hunan, China

**Yina Jia**, MD. Sinopec Engineering Incorporation. Beijing, China.

Submit your manuscript to a SpringerOpen® journal and benefit from:

- Convenient online submission
- Rigorous peer review
- Open access: articles freely available online
- High visibility within the field
- Retaining the copyright to your article

Submit your next manuscript at ► [springeropen.com](https://www.springeropen.com)